Materials Today Physics 29 (2022) 100921

Contents lists available at ScienceDirect

Materials Today Physics

journal homepage: www.journals.elsevier.com/materials-today-physics

Tunable near-field thermal rectifiers by nanostructures

Lin Jing [1], Zhuo Li [1], Hakan Salihoglu, Xiu Liu, Sheng Shen [*]

Department of Mechanical Engineering, Carnegie Mellon University, Pittsburgh, PA, 15213, USA

ARTICLE INFO

Keywords:
Near-field
Thermal rectification
Tunable Nanowire
Nanocross
Vanadium dioxide

ABSTRACT

The capability of manipulating heat flux at the nanoscale has important implications in thermal circuits and thermal management of electronics. In this work, by employing both the fluctuating surface current method and the Wiener-chaos expansion method, we demonstrate a tunable thermal rectification effect based on the near-field radiation for nanowire and nanocross structures. Due to the different decay behaviors of surface phonon polaritons and surface plasmon polaritons, the rectification can be bidirectionally controlled at various rates by tuning the separation between the nanostructures. This work provides new pathways for designing contactless smart thermal modulation devices.

1. Introduction

Recent advances in thermal control and heat regulation render thermal logic devices promising for applications in thermal management of electronics, energy conversion systems, and thermal logic circuits [1–4]. Among existing thermal logic devices (e.g., transistors, memories, and logic gates), thermal rectifiers have attracted significant interest [5]. Analogous to its electronic counterpart, a thermal rectifier is a two-terminal device allowing thermal current to flow preferentially in one direction, either forwardly or backwardly, under a temperature bias. The contrast between the forward and backward heat flows is characterized by a rectification ratio R, which is defined by subtracting 1 from the ratio of the forward and backward heat flows. To realize such an asymmetry in heat transfer, a variety of mechanisms have been explored for developing solid-state rectification devices, including conductive [6–9] and radiative approaches [10,11][45]. The radiative approach employs the temperature dependent optical properties of the two terminals that are typically made from distinct materials. While the two terminals are subject to a favorable temperature bias under which their corresponding electromagnetic resonances are spectrally aligned, strong electromagnetic coupling between the resonances occurs. In contrast, when the temperature bias is reversed, the loss of the resonance coupling will block thermal radiation [10].

Phase change materials are promising candidates for achieving temperature dependent optical properties and thus thermal rectification. Vanadium dioxide (VO_2), known as a typical thermochromic material, experiences metal-insulator transition at a critical temperature, $T_c \sim 340$ K, associated with structural transition [12]. Below the critical temperature, VO_2 exhibits insulating properties with a monoclinic structure. Above T_c, it is in the metallic state with a rutile structure [13]. As a result, the infrared response of VO_2 alters dramatically across the phase transition, showing great promise for developing VO_2-based radiative thermal rectifier in both the far-field and near-field regimes [14–16]. In a recent theoretical study, a rectification ratio >20 can be obtained via matching the VO_2 loss with its host material in a micro-grating structure [17]. Experimentally, the rectification ratio as large as 2 was demonstrated between VO_2 and SiO_2 [18].

In the near-field regime, it is evanescent waves that mainly contribute to the radiative heat transfer [19,20]. Furthermore, when the media support surface polaritons, the evanescent waves stemming from the excitation of surface phonon polaritons (SPhPs) or surface plasmon polaritons (SPPs) will significantly enhance the near-field radiation in comparison with corresponding blackbody radiation [20–29]. In this regard, VO_2 is particularly attractive for tuning near-field radiation as there exist surface phonon modes in the infrared region for the insulating VO_2. Therefore, extensive efforts have been made to investigate the thermal rectification between VO_2 and other interacting materials in the near-field regime. Theoretically [11,30-33] a rectification ratio of one order of magnitude can be achieved when the two semi-infinite terminals are separated by a 10 nm gap [11]. Experimental implementations focusing on plate-plate [5,34] and sphere-plate [35] configurations have been reported. Thus far, the studies on the near-field thermal rectification with phase transition materials have mainly been based on bulk structures and materials, in which the rectification

* Corresponding author.
E-mail address: sshen1@cmu.edu (S. Shen).
[1] These authors contributed equally to this work.

https://doi.org/10.1016/j.mtphys.2022.100921
Received 26 September 2022; Received in revised form 6 November 2022; Accepted 14 November 2022
Available online 15 November 2022

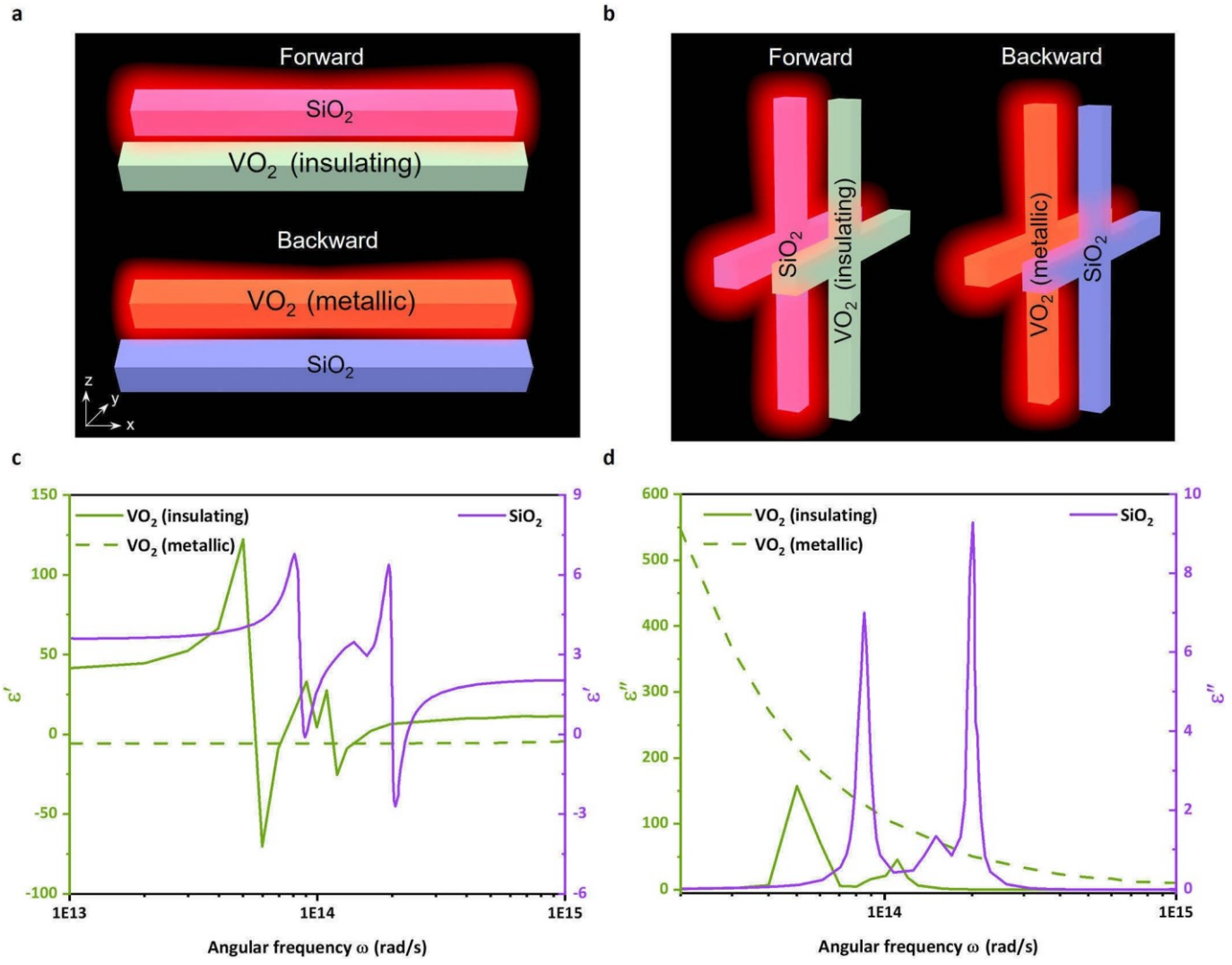

Fig. 1. Schematic diagrams of the thermal rectification model. (a), Nanowire-nanowire configuration. (b), Nanocross-nanocross configuration. (c) and (d), Real and imaginary parts of the dielectric function of VO_2 and SiO_2.

direction (sign of R value) is independent of separation gap under a given temperature bias. Moreover, no tunability in terms of rectification direction has been achieved.

In this work, we demonstrate the near-field thermal rectifiers capable of tailoring rectification directions based on nanowire and nanocross configurations. To study the near-field radiation between nanostructures with one terminal being VO_2 and the other being SiO_2, both the fluctuating surface current (FSC) method and the Wiener-chaos expansion (WCE) method are employed in our direct calculations. Both nanowire and nanocross configurations allow us to bidirectionally manipulate the radiation at different rectification rates by tuning the separation between VO_2 and SiO_2. Particularly, the presence of degenerate modes in nanocross structures, as compared to the corresponding nanowires, can boost the energy density and rectification range.

2. Numerical model

Two configurations including nanowires and nanocrosses are considered in this work, as shown in Fig. 1(a) and (b), respectively. The nanowires and the perpendicular beams in the nanocross structure are 1.5 μm long with a 120 nm × 120 nm square shape cross-section at the separations of 50, 100, 150 and 200 nm, respectively, considering the current nano-fabrication capability and near-field thermal signal sensing competence in real applications. Following the convention [30,31], the forward temperature bias is defined as the scenario where the temperature of SiO_2 is greater than that of VO_2, while the backward bias defines the case with VO_2 having a greater temperature. The high, T_h, and the low, T_l, temperatures are set to be 373 K and 303 K, respectively, which is either above or below the transition temperature of VO_2. Therefore, VO_2 behaves as an insulator in the forward bias but a metal in the backward bias. For the dielectric function of insulating VO_2, a classical oscillator model $\varepsilon_i(\omega) = \varepsilon_\infty + \sum_{j=1}^{N} S_j\omega_j^2 / \left(\omega_j^2 - i\gamma_j\omega - \omega^2\right)$ is adopted, where ε_∞ is the high-frequency constant, ω_j is the phonon vibration frequency, γ_j is the scattering rate, S_j represents the oscillation strength, and j is the mode index. Metallic VO_2 can be approximated by the Drude model $\varepsilon_m(\omega) = -\omega_p^2\varepsilon_\infty/(\omega^2 - i\omega\Upsilon)$, where ε_∞ is a constant, ω_p and Υ represent the plasma frequency and the collision frequency, respectively. The fitting parameters can be found in Ref. [36] for the insulating phase and Ref. [31] for the metallic phase. The dielectric property of SiO_2 is given by Palik [37]. As demonstrated in Fig. 1(c) and (d), the dielectric behaviors of insulating VO_2 and SiO_2 show overlapped phonon resonances, whereas the metallic VO_2 only manifests the Drude type absorption.

We exploit the FSC method to model the radiative heat transfer between nanowires or nanocrosses because it enables the high-efficiency

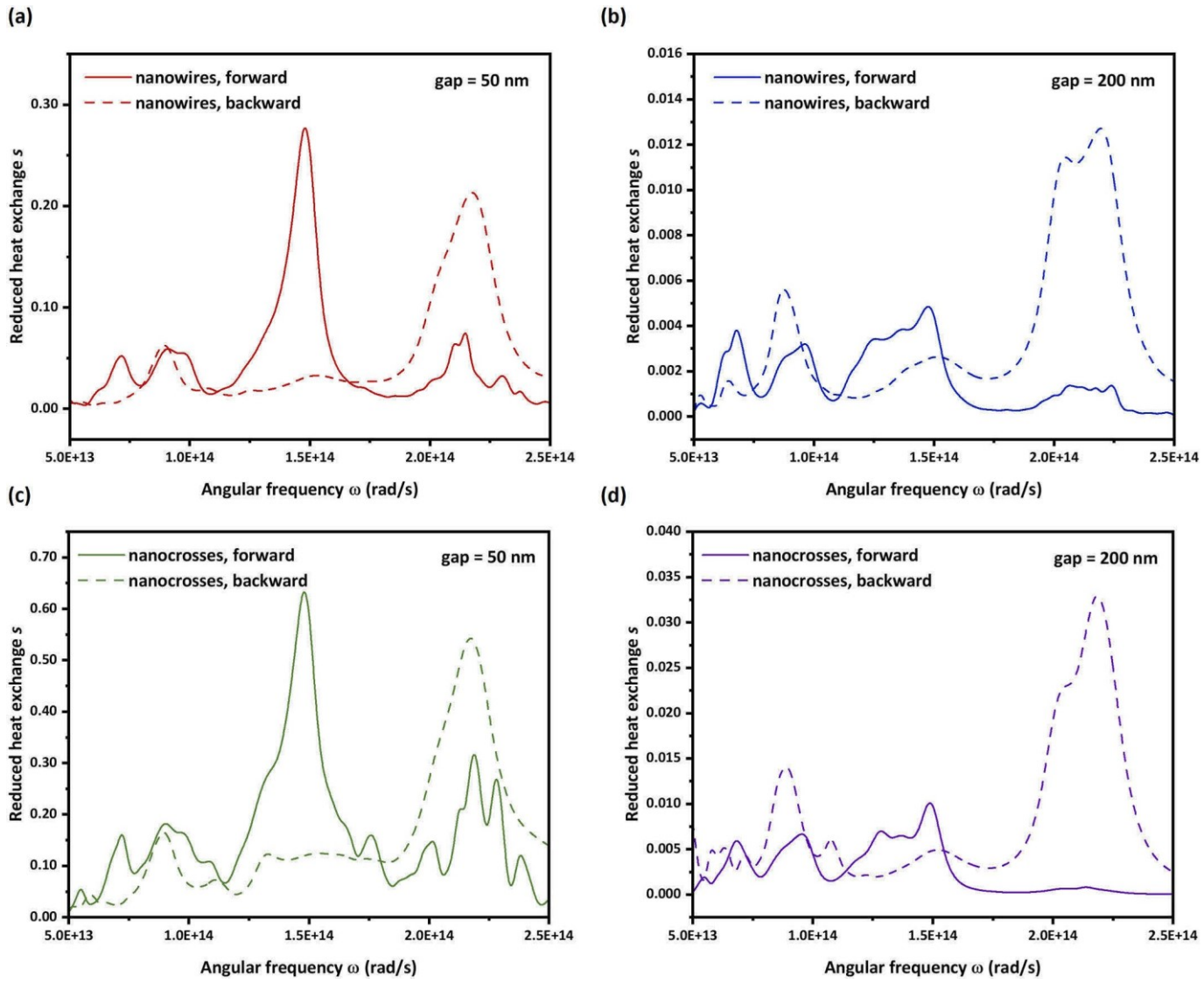

Fig. 2. Reduced heat exchange spectra $s(\omega)$ in both the forward (solid lines) and the backward (dashed lines) directions between (a)–(b) a pair of nanowires, and (c)–(d) nanocrosses. The gaps are 50 nm for panels (a) and (c), and 200 nm for panels (b) and (d), respectively.

thermal radiation calculation between arbitrary geometries [38–40]. When simulating the electromagnetic response of a structure due to thermally induced fluctuating currents, the equivalent surface currents on the surface boundary serve as the source to the stochastic Maxwell's equation where the homogenous Dyadic Green's function is involved in calculating the real electromagnetic response. The computation based on the FSC method yields the exchange function $s(\omega)$, also known as the reduced spectral heat exchange. Detailed derivations have been reported by other authors in Refs. [38–40], herein, only key equations are presented in Supplementary Materials Note S1. Accordingly, the net radiative heat transfer between the two terminals at temperatures of T_h and T_l can be obtained as:

$$q = \int_0^\infty [\Theta(\omega, T_h) - \Theta(\omega, T_l)]s(\omega)d\omega, \quad (1)$$

where $\Theta(\omega, T_i) = \hbar\omega/[\exp(\hbar\omega/k_B T_i - 1)]$ for $i \in \{h, l\}$, is the energy of a Planck oscillator at the angular frequency ω in thermal equilibrium at temperature T_i. The boundary meshing size in the calculation is 30 nm, which is determined by a thorough mesh independence study. To verify the accuracy of the FSC method used in this study, the simulation results for the spectral radiation between two sufficiently large and thick plates are compared with that of semi-infinite planes reported in Ref. [31]. With the net heat flows for the forward-biased, q_f, and backward-biased, q_b, cases, the rectification ratio R is then defined as:

$$R \equiv \frac{q_f}{q_b} - 1. \quad (2)$$

Correspondingly, $R > 0$ indicates a greater forward heat flow, and there is rectification in the forward direction, whereas the rectification direction is reversed if $R < 0$.

3. Results and discussion

In Fig. 2(a) and (b), we show the two representative reduced heat exchanges $s(\omega)$ for nanowires with separations of 50 nm and 200 nm, respectively, while the results for nanocrosses are plotted in Fig. 2(c) and (d). Results corresponding to other gap distances (100 nm and 150 nm) can be found in Supplementary Materials Fig S2.

As shown in Fig. 2(a) and (b), the reduced heat exchange spectra of a pair of nanowires in the forward and backward biases are dominated by different modes. In the forward cases, the near-field radiation spectra are mainly dominated by the peaks around 1.5×10^{14} rad/s, where the real parts of permittivity for both SiO_2 and insulating VO_2 are close to

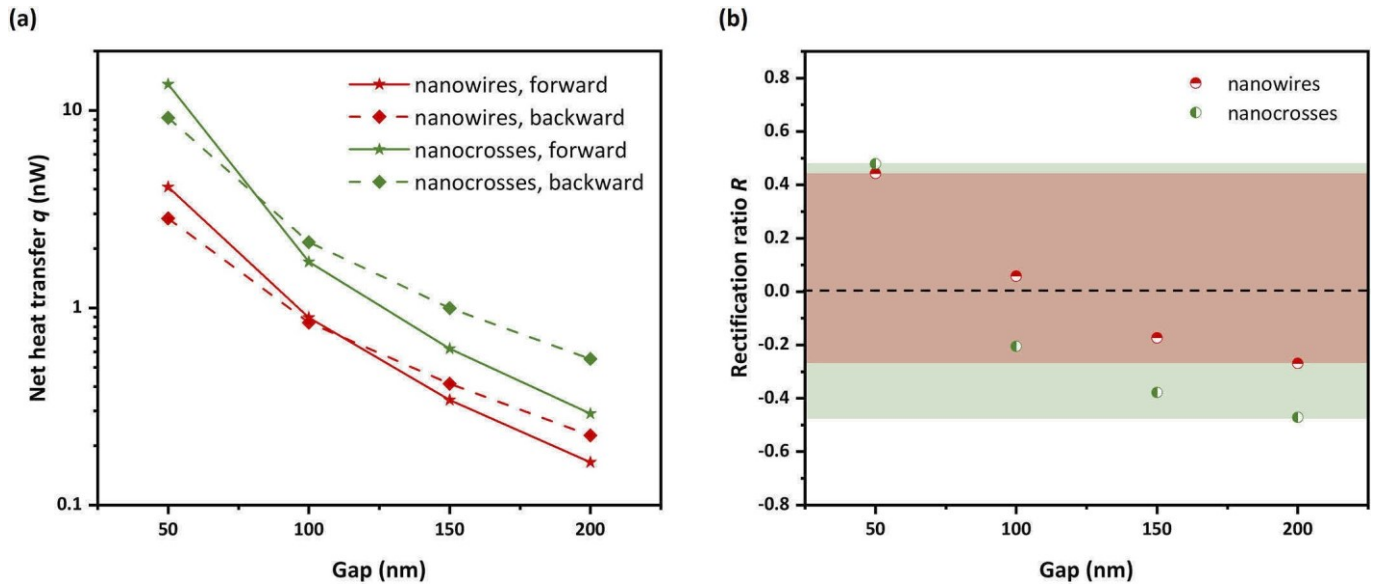

Fig. 3. (a). Net heat transfer between a pair of nanowires (red lines) and nanocrosses (green lines) in both the forward (solid lines) and the backward (dashed lines) cases at different gaps. (b). Rectification ratios of the nanowire structures (red dots) and the nanocross structures (green dots) at different gaps; the red and green shadows show the corresponding rectification ranges. (For interpretation of the references to colour in this figure legend, the reader is referred to the Web version of this article.)

−1 (Fig. 1(c)), corresponding to the excitation of SPhPs. In addition, near the same frequency, SiO_2 also has a minor peak in the imaginary part of its permittivity (Fig. 1(d)), indicating relatively strong absorption. Therefore, SPhP-induced electromagnetic coupling facilitates the near-field radiative heat transfer between SiO_2 and insulating VO_2 nanowires, leading to the peak around 1.5×10^{14} rad/s. In contrast,

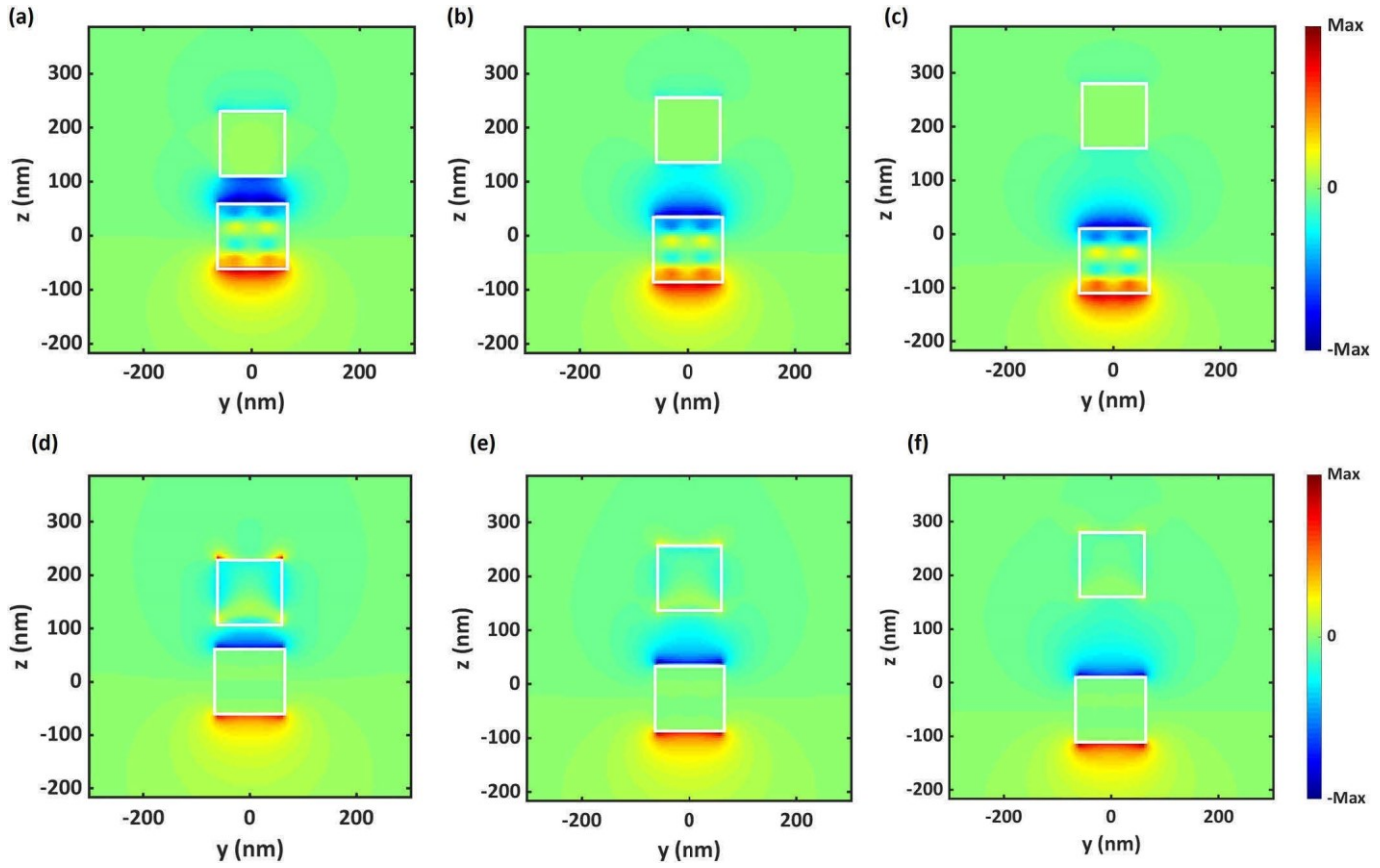

Fig. 4. E_z field profiles in the nanowire-nanowire configuration at various gaps. (a)−(c), The forward cases with the gaps of 50 nm, 100 nm, and 150 nm, respectively. (d)−(f), The backward cases with the gaps of 50 nm, 100 nm, and 150 nm, respectively. The field profiles are captured at the ends of the nanowires at corresponding resonance frequencies. The white lines highlight the cross-sections of the structures. In each panel, emissions are excited from the bottom structure.

in the backward cases, the near-field heat transfer is dominated by the peak located at 2.2×10^{14} rad/s, which corresponds to the SPP modes supported by the longitudinal oscillation of charges inside the VO_2 nanowire in the metallic phase.

These SPhP and SPP modes, however, exhibit different spatial decays from the emitter surface. At small separations (e.g., 50 nm), the peak in the forward case driven by SPhPs is higher than that in the backward case driven by SPP modes, as shown in Fig. 2(a). However, the SPhP modes tend to decay with a higher rate from the emitter than the SPP modes. Thus, the SPP will dominate in the large-gap cases, as indicated by the comparison of the respective peaks in Fig. 2(a) and (b). This causes the backward net heat flow to outperform that in the forward direction for the gap distances larger than 100 nm, which leads to the reverse of the rectification direction (change in the sign of R), as shown in Fig. 3.

Due to the rotational symmetry of nanocrosses, they can support two degenerate modes (one along each arm). In the far-field regime [41], the existence of uncoupled degenerate modes only doubles the peak height in the radiation spectrum. However, the coupling between the two degenerate modes provides extra channels for enhancing radiative heat transfer in the near-field, as discussed in our previous work [42]. In consequence, nanocrosses enable higher near-field radiation as compared with nanowires. As the SPhP modes show a higher spatial decay rate, a negative rectification is achieved at larger gap distances for nanocross structures as well. Based on the reduced heat exchange spectra, the net energy transfer between the nanostructures can then be calculated from Eq. (1) as a function of gap distances (Fig. 3(a)). Accordingly, the rectification ratios are obtained by Eq. (2), as shown in Fig. 3(b).

As observed from the net heat transfer in Fig. 3(a), the backward net heat transfer of both nanowires and nanocrosses decreases with a lower rate when increasing separations and exceeds the forward ones after separation >100 nm, leading to the reverse of the rectification direction. Furthermore, in both the directions, the net heat transfer between nanocrosses deviates from two times of that between nanowires given the same gap, which can be attributed to the coupling of degenerate modes. Such the coupling in the nanocrosses also leads to larger rectification, compared to the nanowire structures. In Fig. 3(b), by varying the gap distances from 50 nm to 200 nm, the rectification ratio of the nanocross structures ranges from 0.48 to −0.47, comparing to a relatively narrower range from 0.44 to −0.27 for the nanowire structures. Nevertheless, both the nanowire and nanocross structures realize negative rectification ratios for the gap distances larger than 100 nm, which has never been accomplished in previous studies [10,31,33].

To better understand such a bidirectional rectification behavior with respect to separation, we plot the mode profiles of nanowire configuration under different separations to compare the decay rates of the supported SPhP and SPP modes. In Fig. 4, we show the E_z profiles captured at the ends of the two nanowires with selected gap distances for both the directions. The field profiles are simulated via the WCE method [43,44], where a series of dipoles (a number of $20 \times 2 \times 2$ in $x \times y \times z$ directions, respectively) are added to the emitter according to a set of deterministic base functions to systematically excite the supported modes. Due to the confinement of the nanowires in the y direction, the SPhP modes supported in the forward direction (Fig. 4(a)–(c)) are more localized at the top two edges along the SiO_2 nanowire (top left and right corners in the y-z plots) because of reflection/scattering at the edges, which causes the mode profiles spreading in the y-z plane. Such a spreading results in the dramatic decrease of the field intensity along the z direction from the top surface of the emitter (bottom white boxes), indicating that the SPhP modes significantly attenuate within the gap. However, in the backward direction, the SPP modes supported by the metallic phase of VO_2 (Fig. 4(d)–(f)) are distributed more uniformly on the top surface of emitter, leading to a more directional mode profile and a relatively lower decay rate. The reverse of the rectification direction of the nanocross structures can be understood under the same principle because they share the same dominant modes as nanowires. Here, different from the conventional surface modes supported by an infinitely large surface (see Supplementary Materials Note S2 for the corresponding results of the semi-infinite plate configuration), the mode profiles and thus the bidirectional rectification effect highly depend on the different localizations of SPhP and SPP modes to the nanowire cross-sections. Varying the shape and size of the nanowire cross-section or introducing cross-sectional asymmetry endows the bidirectional rectification behavior with great tailorability. In other words, the gap distances where the reversed rectification occurs can be designed in a flexible manner.

4. Conclusions

In conclusion, by exploiting nanowire and nanocross structures with phase transition material in the near-field regime, we have observed a tunable thermal rectification phenomenon. By tuning separation between nanostructures, the rectification can be bidirectionally tailored at different rates. Specifically, when the nanowires made of SiO_2 and VO_2 are separated by small gaps (e.g., <100 nm), the strong coupling of localized SPhP modes between SiO_2 and VO_2 in the insulating state induces enhanced near-field radiative transfer which outperforms that when VO_2 is metallic. However, as the separation enlarges, the SPhPs mediated radiative heat transfer is surpassed by the case of the SPPs between the metallic VO_2 and SiO_2, leading to the reverse rectification. Due to the coupling of degenerate modes, the nanocross-based thermal rectifier reveals superior near-field radiation capability and broader rectification tunability as compared to the nanowire configuration. Such bidirectional thermal rectification provides an extra degree of freedom in manipulating the near-field radiative heat transfer and opens a new avenue for the future design of contactless thermal logic devices.

Credit author statement

Lin Jing: Conceptualization, Investigation, Formal analysis, Validation, Writing - Original Draft, Visualization. **Zhuo Li:** Methodology, Investigation, Formal analysis, Validation, Writing - Original Draft. **Hakan Salihoglu:** Formal analysis, Writing - Review & Editing. **Xiu Liu:** Writing - Review & Editing. **Sheng Shen:** Supervision.

Declaration of competing interest

The authors declare that they have no known competing financial interests or personal relationships that could have appeared to influence the work reported in this paper.

Data availability

Data will be made available on request.

Acknowledgements

Lin Jing and Zhuo Li identified the problem. Lin Jing performed the numerical simulation. Zhuo Li, Hakan Salihoglu and Lin Jing conducted the physical analysis. Lin Jing and Zhuo Li wrote the paper with the input and revisions from all the authors. Sheng Shen supervised the research. All authors have given consent to the final version of the paper.

The authors are grateful to the Defense Threat Reduction Agency (Grant No. HDTRA1-19-1-0028) and the National Science Foundation (Grant No. CBET-1931964).

Appendix A. Supplementary data

Supplementary data to this article can be found online at https://doi.org/10.1016/j.mtphys.2022.100921.

References

[1] R. Scheibner, M. Kȍnig, D. Reuter, A.D. Wieck, C. Gould, H. Buhmann, L. W. Molenkamp, Quantum dot as thermal rectifier, New J. Phys. 10 (8) (2008): 083016.

[2] W. Kobayashi, Y. Teraoka, I. Terasaki, An oxide thermal rectifier, Appl. Phys. Lett. 95 (17) (2009): 171905.

[3] D. Sawaki, W. Kobayashi, Y. Moritomo, I. Terasaki, Thermal rectification in bulk materials with asymmetric shape, Appl. Phys. Lett. 98 (8) (2011): 081915.

[4] P. Ben-Abdallah, S.-A. Biehs, Near-field thermal transistor, Phys. Rev. Lett. 112 (4) (2014): 044301.

[5] M. Elzouka, S. Ndao, High temperature near-field NanoThermoMechanical rectification, Sci. Rep. 7 (1) (2017): 44901.

[6] R. Shrestha, Y. Luan, X. Luo, S. Shin, T. Zhang, P. Smith, W. Gong, M. Bockstaller, T. Luo, R. Chen, K. Hippalgaonkar, S. Shen, Dual-mode solid-state thermal rectification, Nat. Commun. 11 (1) (2020) 4346.

[7] C.W. Chang, D. Okawa, A. Majumdar, A. Zettl, Solid-state thermal rectifier, Science 314 (5802) (2006) 1121–1124.

[8] B. Li, L. Wang, G. Casati, Thermal diode: rectification of heat flux, Phys. Rev. Lett. 93 (18) (2004): 184301.

[9] A. Aiyiti, Z. Zhang, B. Chen, S. Hu, J. Chen, X. Xu, B. Li, Thermal rectification in Y-junction carbon nanotube bundle, Carbon 140 (2018) 673–679.

[10] C.R. Otey, W.T. Lau, S. Fan, Thermal rectification through vacuum, Phys. Rev. Lett. 104 (15) (2010): 154301.

[11] J. Huang, Q. Li, Z. Zheng, Y. Xuan, Thermal rectification based on thermochromic materials, Int. J. Heat Mass Tran. 67 (2013) 575–580.

[12] F.J. Morin, Oxides which show a metal-to-insulator transition at the neel temperature, Phys. Rev. Lett. 3 (1) (1959) 34–36.

[13] Z. Shao, X. Cao, H. Luo, P. Jin, Recent progress in the phase-transition mechanism and modulation of vanadium dioxide materials, NPG Asia Mater. 10 (7) (2018) 581–605.

[14] E. Nefzaoui, K. Joulain, J. Drevillon, Y. Ezzahri, Radiative thermal rectification using superconducting materials, Appl. Phys. Lett. 104 (10) (2014): 103905.

[15] A. Ghanekar, G. Xiao, Y. Zheng, High contrast far-field radiative thermal diode, Sci. Rep. 7 (1) (2017) 6339.

[16] P. Ben-Abdallah, S.-A. Biehs, Phase-change radiative thermal diode, Appl. Phys. Lett. 103 (19) (2013): 191907.

[17] R. Audhkhasi, M.L. Povinelli, Design of far-field thermal rectifiers using gold–vanadium dioxide micro-gratings, J. Appl. Phys. 126 (6) (2019): 063106.

[18] K. Ito, K. Nishikawa, H. Iizuka, H. Toshiyoshi, Experimental investigation of radiative thermal rectifier using vanadium dioxide, Appl. Phys. Lett. 105 (25) (2014): 253503.

[19] Z.M. Zhang, Nano/Microscale Heat Transfer; Mechanical Engineering Series, Springer International Publishing, Cham, 2020.

[20] C.J. Fu, Z.M. Zhang, Nanoscale radiation heat transfer for silicon at different doping levels, Int. J. Heat Mass Tran. 49 (9–10) (2006) 1703–1718.

[21] S. Shen, A. Narayanaswamy, G. Chen, Surface phonon polaritons mediated energy transfer between nanoscale gaps, Nano Lett. 9 (8) (2009) 2909–2913.

[22] E. Rousseau, A. Siria, G. Jourdan, S. Volz, F. Comin, J. Chevrier, J.-J. Greffet, Radiative heat transfer at the nanoscale, Nat. Photonics 3 (9) (2009) 514–517.

[23] R.S. Ottens, V. Quetschke, S. Wise, A.A. Alemi, R. Lundock, G. Mueller, D.H. Reitze, D.B. Tanner, B.F. Whiting, Near-field radiative heat transfer between macroscopic planar surfaces, Phys. Rev. Lett. 107 (1) (2011): 014301.

[24] X.L. Liu, Z.M. Zhang, Graphene-assisted near-field radiative heat transfer between corrugated polar materials, Appl. Phys. Lett. 104 (25) (2014): 251911.

[25] J. Shi, P. Li, B. Liu, S. Shen, Tuning near field radiation by doped silicon, Appl. Phys. Lett. 102 (18) (2013): 183114.

[26] J. Li, B. Liu, S. Shen, Graphene surface plasmons mediated thermal radiation, J. Opt. 20 (2) (2018): 024011.

[27] B. Liu, Y. Liu, S. Shen, Thermal plasmonic interconnects in graphene, Phys. Rev. B 90 (19) (2014): 195411.

[28] J. Li, Z. Li, X. Liu, S. Maslovski, S. Shen, Active control of thermal emission by graphene-nanowire coupled plasmonic metasurfaces, Phys. Rev. B 106 (11) (2022): 115416.

[29] E. Andrade, R. Carrillo-Bastos, P.A. Pantaleón, F. Mireles, Resonant transport in kekulé-distorted graphene nanoribbons, J. Appl. Phys. 127 (5) (2020): 054304.

[30] P.J. Van Zwol, K. Joulain, P. Ben-Abdallah, J. Chevrier, Phonon polaritons enhance near-field thermal transfer across the phase transition of VO 2, Phys. Rev. B 84 (16) (2011): 161413.

[31] Y. Yang, S. Basu, L. Wang, Radiation-based near-field thermal rectification with phase transition materials, Appl. Phys. Lett. 103 (16) (2013): 163101.

[32] F. Chen, X. Liu, Y. Tian, Y. Zheng, Dynamic tuning of near–field radiative thermal rectification, Adv. Eng. Mater. 23 (2) (2021): 2000825.

[33] L.P. Wang, Z.M. Zhang, Thermal rectification enabled by near-field radiative heat transfer between intrinsic silicon and a dissimilar material, Nanoscale Microscale Thermophys. Eng. 17 (4) (2013) 337–348.

[34] A. Fiorino, D. Thompson, L. Zhu, R. Mittapally, S.-A. Biehs, O. Bezencenet, N. El-Bondry, S. Bansropun, P. Ben-Abdallah, E. Meyhofer, P. Reddy, A thermal diode based on nanoscale thermal radiation, ACS Nano 12 (6) (2018) 5774–5779.

[35] P.J. Van Zwol, L. Ranno, J. Chevrier, Tuning near field radiative heat flux through surface excitations with a metal insulator transition, Phys. Rev. Lett. 4 (2012).

[36] A.S. Barker, H.W. Verleur, H.J. Guggenheim, Infrared optical properties of vanadium dioxide above and below the transition temperature, Phys. Rev. Lett. 17 (26) (1966) 1286–1289.

[37] E.D. Palik, Handbook of Optical Constants of Solids, vol. 3, Academic press, 1998.

[38] A.W. Rodriguez, M.T.H. Reid, S.G. Johnson, Fluctuating-surface-current formulation of radiative heat transfer for arbitrary geometries, Phys. Rev. B 86 (22) (2012): 220302.

[39] A.W. Rodriguez, M.T.H. Reid, S.G. Johnson, Fluctuating-surface-current formulation of radiative heat transfer: theory and applications, Phys. Rev. B 88 (5) (2013): 054305.

[40] J. Li, Thermal Radiation from Nanophotonic Structures: Theory, Numerical Simulation and Applications, Carnegie Mellon University, 2020.

[41] L. Zhu, S. Sandhu, C. Otey, S. Fan, M.B. Sinclair, T. Shan Luk, Temporal coupled mode theory for thermal emission from a single thermal emitter supporting either a single mode or an orthogonal set of modes, Appl. Phys. Lett. 102 (10) (2013): 103104.

[42] J. Li, Z. Li, S. Shen, Degenerate quasi-normal mode theory for near-field radiation between plasmonic structures, Opt Express 28 (23) (2020): 34123.

[43] Z. Li, J. Li, X. Liu, H. Salihoglu, S. Shen, Wiener chaos expansion method for thermal radiation from inhomogeneous structures, Phys. Rev. B 104 (19) (2021): 195426.

[44] J. Li, B. Liu, S. Shen, Tunable narrow-band near-field thermal emitters based on resonant metamaterials, Phys. Rev. B 96 (7) (2017): 075413.

[45] Yong Zhang, Chenglong Zhou, Hongliang Yi, Heping Tan, Radiative thermal diode mediated by nonreciprocal graphene plasmon waveguides, Physical Review Applied 13 (3) (2020) 034021.